

On the Construction, Comparison, and Local Characteristic Decomposition for High Order Central WENO Schemes

Jianxian Qiu¹ and Chi-Wang Shu²

ABSTRACT

In this paper, we first construct fourth and eighth order central WENO (weighted essentially non-oscillatory) schemes based on a finite volume formulation, staggered mesh, and continuous extension of Runge-Kutta methods, for solving nonlinear hyperbolic conservation law systems. Negative linear weights appear in such a formulation and they are treated using the technique recently introduced by Shi, Hu and Shu [19]. We then perform numerical computations and comparisons with finite difference WENO schemes of Jiang and Shu [5] and Balsara and Shu [1]. The emphasis is on the performance with or without a local characteristic decomposition. While this decomposition increases the computational cost, we demonstrate by our numerical experiments that it is still necessary to use it to remove spurious oscillations when the order of accuracy is high, both for the central staggered grid and for the upwind non-staggered grid WENO schemes. We use the shock entropy wave interaction problem to demonstrate the advantage of using a higher order WENO schemes when both shocks and complex solution features co-exist.

Key Words: WENO scheme, central scheme, high order accuracy, local characteristic decomposition.

AMS(MOS) subject classification: 65M06, 65M99, 35L65

¹Department of Mathematics, University of Science and Technology of China, Hefei, Anhui 230026, P.R. China. E-mail: jxqiu@ustc.edu.cn. The research of this author is supported in part by NSFC grant 59979004 and 10028103.

²Division of Applied Mathematics, Brown University, Providence, RI 02912, USA. E-mail: shu@cfm.brown.edu. The research of this author is supported in part by NSFC grant 10028103 while he is in residence at the Department of Mathematics, University of Science and Technology of China, Hefei, Anhui 230026, P.R. China. Additional support is provided by ARO grant DAAD19-00-1-0405 and NSF grant DMS-9804985.

1 Introduction

In this paper, we first construct fourth and eighth order central WENO (weighted essentially non-oscillatory) schemes based on a finite volume formulation, staggered mesh, and continuous extension of Runge-Kutta methods, for solving nonlinear hyperbolic conservation law systems

$$\begin{cases} u_t + \nabla \cdot f(u) = 0 \\ u(x, 0) = u_0(x) \end{cases} \quad (1.1)$$

Only the one dimensional case is considered in this paper, although the algorithm can be extended to multi-dimensions along the lines of [6, 7, 10, 12]. Negative linear weights appear in such a formulation and they are treated using the technique recently introduced by Shi, Hu and Shu [19]. We then perform numerical computations and comparisons with finite difference WENO schemes of Jiang and Shu [5] and Balsara and Shu [1]. The emphasis is on the performance with or without a local characteristic decomposition. While this decomposition increases the computational cost, we demonstrate by our numerical experiments that it is still necessary to use it to remove spurious oscillations when the order of accuracy is high, both for the central staggered grid or upwind non-staggered grid WENO schemes. We use the shock entropy wave interaction problem to demonstrate the advantage of using a higher order WENO schemes when both shocks and complex solution features co-exist.

The central schemes are extensions of the Lax-Friedrichs (LxF) scheme. The LxF scheme is very simple and robust, but it is only first order accurate and excessively diffusive. In 1990 Nessyahu and Tadmor [17] developed a class of non-oscillatory second-order central difference approximations to hyperbolic conservation laws in one spatial dimension (the NT schemes). These approximations can be viewed as a natural extension of the LxF scheme and can be proven TVD (total variation diminishing) in the scalar one dimensional case. For the system case, these second order central schemes require no Riemann solvers, no local characteristic decompositions and no flux splitting. Therefore, all that one has to do in order to solve (1.1) is to supply the flux function $f(u)$. Thus the NT central schemes are simpler than most

upwind schemes (they are comparable in simplicity and cost with upwind schemes using a Lax-Friedrichs building block and componentwise limiting or ENO/WENO reconstruction), especially for cases where the complete set of eigenvectors of the Jacobian $f'(u)$ are difficult to obtain or they simply do not exist (such as for the weakly hyperbolic systems). For these reasons NT schemes and their extensions have become quite popular in applications. After the pioneer work of Nessyahu and Tadmor in [17], many different central schemes have been developed [6, 7, 9, 15, 18, 2, 8, 10, 11, 12]. A major difference between different central schemes is in the reconstruction step, where one computes a piecewise polynomial interpolation from the cell-averages. The second order NT scheme [17] and its extension to 2D [6, 7] are based on a MUSCL-like piecewise linear interpolant and nonlinear limiters to prevent spurious oscillations; the third-order scheme by Liu and Tadmor [15] are based on a quadratic interpolant developed by Liu and Osher [14]; the third-order and fourth-order schemes by Bianco et al. [2] are based on a modified ENO reconstruction of point values from cell averages, and on numerical fluxes on cell boundaries. The reconstruction of the x-derivatives of $f(u)$ is performed from interpolation of grid values of $f(u)$, and the evaluation of the fluxes is obtained through a Runge-Kutta method with the aid of the so-called natural continuous extension (NCE) [24]. The usage of this NCE Runge-Kutta technique gives great flexibility at low computational cost. In the spirit of Godunov-type schemes, Levy et al. [10, 12] present a third-order central scheme for approximating solutions of systems of conservation laws in one and two space dimensions. The method is based on reconstructing a piecewise-polynomial interpolant from cell-averages which is then advanced in time. In the reconstruction step, a third-order, compact, central weighted essentially nonoscillatory (CWENO) reconstruction is introduced, which is written as a convex combination of interpolants based on different stencils. In the one-dimensional case, the third-order reconstruction is based on an extremely compact three-point stencil. Analogous compactness is retained in more space dimensions. In contrast to NT scheme based on cell averages, schemes by Liu and Osher [13] are based on point values and the general ENO philosophy, removing the need for staggered grids thus

getting rid of the associated difficulties at the boundary.

The first WENO scheme is constructed in [16] for a third order finite volume version in one space dimension. In [5], third and fifth order finite difference WENO schemes in multi space dimensions are constructed, with a general framework for the design of the smoothness indicators and nonlinear weights. WENO schemes are designed based on the successful ENO schemes in [3, 22, 23]. Both ENO and WENO schemes use the idea of adaptive stencils in the reconstruction procedure based on the local smoothness of the numerical solution to automatically achieve high order accuracy and non-oscillatory property near discontinuities. ENO uses just one (optimal in some sense) out of many candidate stencils when doing the reconstruction; while WENO uses a convex combination of all the candidate stencils, each being assigned a nonlinear weight which depends on the local smoothness of the numerical solution based on that stencil. WENO improves upon ENO in robustness, better smoothness of fluxes, better steady state convergence, better provable convergence properties, and more efficiency. Third and fourth order triangle based finite volume WENO schemes can be found in [4]. For a detailed review of ENO and WENO schemes, we refer to the lecture notes [21]. WENO schemes have already been widely used in applications.

A key idea in WENO schemes is a linear combination of lower order fluxes or reconstruction to obtain a higher order approximation. The combination coefficients, also called linear weights, are determined by local geometry of the mesh and order of accuracy and may become negative. WENO procedures cannot be applied directly to obtain a stable scheme if negative linear weights are present. Previous strategy for handling this difficulty is by either regrouping of stencils or reducing the order of accuracy to get rid of the negative linear weights. In [19], Shi, Hu and Shu presented a simple and effective technique for handling negative linear weights without a need to get rid of them. This technique is used in our work for designing fourth and eighth order central WENO schemes.

The organization of this paper is as follows. In section 2 we construct fourth and eighth order CWENO (central weighted essentially non-oscillatory) schemes based on a finite volume

formulation, staggered mesh, and continuous extension of Runge-Kutta methods, for solving one dimensional nonlinear hyperbolic conservation laws. In section 3 we perform numerical computations and comparisons with finite difference WENO schemes of Jiang and Shu [5] and Balsara and Shu [1]. The emphasis is on the performance with or without a local characteristic decomposition. We also use the shock entropy wave interaction problem to demonstrate the advantage of using a higher order WENO schemes when both shocks and complex solution features co-exist. Concluding remarks are given in section 4.

2 Fourth and eighth order central WENO schemes

In this section we consider one dimensional conservation laws

$$u_t + f(u)_x = 0. \quad (2.1)$$

For simplicity, we assume that the grid points $\{x_i\}$ are uniform with $x_{i+1} - x_i = h$, and $x_{i+\frac{1}{2}} = \frac{1}{2}(x_i + x_{i+1})$. We also denote the cells $I_i = [x_{i-\frac{1}{2}}, x_{i+\frac{1}{2}}]$, $I_{i+\frac{1}{2}} = [x_i, x_{i+1}]$. Let k be the time step, $t^{n+1} = t^n + k$, $u_i^n = u(x_i, t^n)$ denotes the point values, and $\bar{u}_i^n = \frac{1}{h} \int_{I_i} u(x, t^n) dx$, $\bar{u}_{i+\frac{1}{2}}^n = \frac{1}{h} \int_{I_{i+\frac{1}{2}}} u(x, t^n) dx$ represent the cell averages at time t^n on the cells I_i and $I_{i+\frac{1}{2}}$, respectively. The CWENO scheme approximates the cell averages at time t^{n+1} based on their values at time t^n with staggered space grids. Let us follow [17], integrate (2.1) over the region $I_{i+\frac{1}{2}} \times [t^n, t^{n+1}]$, to get an equivalent formulation of the conservation laws (2.1):

$$\bar{u}_{i+\frac{1}{2}}^{n+1} = \bar{u}_{i+\frac{1}{2}}^n - \frac{1}{h} \left[\int_{t^n}^{t^{n+1}} f(u(x_{i+1}, t)) dt - \int_{t^n}^{t^{n+1}} f(u(x_i, t)) dt \right] \quad (2.2)$$

This finite volume formulation expresses the precise relation between the sliding averages and the underlying point values. We will use this formulation (2.2) as the starting point for the construction of high order CWENO schemes. What we want to do is to find approximations of the cell averages $\bar{u}_{i+\frac{1}{2}}^n$ and the two integrals in (2.2). Thus the algorithm consists of two major steps to evolve from $\{\bar{u}_i^n\}$ to $\{\bar{u}_{i+\frac{1}{2}}^n\}$:

Step 1. The approximation of $\bar{u}_{i+\frac{1}{2}}^n$ from the knowledge of $\{\bar{u}_i^n\}$ by a WENO reconstruction.

Notice that

$$\bar{u}_{i+\frac{1}{2}}^n = \frac{1}{h} \int_{x_i}^{x_{i+1}} u(x, t^n) dx = \frac{1}{h} \left[\int_{x_i}^{x_{i+\frac{1}{2}}} u(x, t^n) dx + \int_{x_{i+\frac{1}{2}}}^{x_{i+1}} u(x, t^n) dx \right],$$

hence we only need to reconstruct $\frac{1}{h} \int_{x_{i-\frac{1}{2}}}^{x_i} u(x, t^n) dx$ for all i because

$$\frac{1}{h} \int_{x_i}^{x_{i+\frac{1}{2}}} u(x, t^n) dx = \bar{u}_i^n - \frac{1}{h} \int_{x_{i-\frac{1}{2}}}^{x_i} u(x, t^n) dx \quad (2.3)$$

by conservation. This step is achieved in the following substeps:

1. We identify r small stencils $S_j, j = 0, \dots, r-1$, such that I_i belongs to each of them. Here we set $S_j = \cup_{l=0}^{r-1} I_{i+j-l}$. We denote by $\mathcal{T} = \cup_{j=0}^{r-1} S_j$ the larger stencil which contains all the cells from the r smaller stencils.
2. We have a $(r-1)$ -th degree polynomial reconstruction denoted by $p_j(x)$, associated with each of the stencils $S_j, j = 0, \dots, r-1$, such that the cell average of $p_j(x)$ in each of the cells in the stencil S_j agrees with the given cell average of u , i.e. $\frac{1}{h} \int_{I_{i+j-l}} p_j(x) dx = \bar{u}_{i+j-l}, l = 0, \dots, r-1$. We also have a higher order $(2r-2)$ -th degree polynomial reconstruction denoted by $Q(x)$, associated with the larger stencil \mathcal{T} , such that $\frac{1}{h} \int_{I_{i+l}} Q(x) dx = \bar{u}_{i+l}, l = -r+1, \dots, r-1$. The detail of the construction of $p_j(x)$ and $Q(x)$ can be found in [21].
3. We find the combination coefficients, also called linear weights, denoted by $\gamma_0, \dots, \gamma_{r-1}$, such that

$$\int_a^b Q(x) dx = \sum_{j=0}^{r-1} \gamma_j \int_a^b p_j(x) dx \quad (2.4)$$

for all possible given cell averages of u in the stencils. These linear weights depend on the mesh geometry and integral interval $[a, b]$, but not on the given solution u in the stencils.

Here in order to compute the approximation of $\frac{1}{h} \int_{x_i}^{x_{i+\frac{1}{2}}} u(x, t^n) dx$ or $\frac{1}{h} \int_{x_{i-\frac{1}{2}}}^{x_i} u(x, t^n) dx$, we can just set $[a, b] = [x_i, x_{i+\frac{1}{2}}]$ or $[a, b] = [x_{i-\frac{1}{2}}, x_i]$. For example, when $r = 3$ and 5,

we have

$$\int_{x_{i-\frac{1}{2}}}^{x_i} p_j(x)dx = \sum_{l=0}^{r-1} a_{jl}\bar{u}_{i+j+l-r+1}, \quad j = 0, \dots, r-1 \quad (2.5)$$

with

$$A = (a_{jl})_{3 \times 3} = \begin{pmatrix} -\frac{1}{16} & \frac{1}{4} & \frac{5}{16} \\ \frac{1}{16} & \frac{1}{2} & -\frac{1}{16} \\ \frac{11}{16} & -\frac{1}{4} & \frac{1}{16} \end{pmatrix}$$

$$\gamma_0 = \frac{3}{16}, \quad \gamma_1 = \frac{5}{8}, \quad \gamma_2 = \frac{3}{16}$$

for $r = 3$, and

$$A = (a_{jl})_{5 \times 5} = \begin{pmatrix} \frac{7}{256} & -\frac{19}{128} & \frac{11}{32} & -\frac{61}{128} & \frac{193}{256} \\ -\frac{3}{256} & \frac{9}{128} & -\frac{13}{64} & \frac{79}{128} & \frac{7}{256} \\ \frac{3}{256} & -\frac{11}{128} & \frac{1}{2} & \frac{11}{128} & -\frac{3}{256} \\ -\frac{7}{256} & \frac{49}{128} & \frac{13}{64} & -\frac{9}{128} & \frac{3}{256} \\ \frac{63}{256} & \frac{61}{128} & -\frac{11}{32} & \frac{19}{128} & -\frac{7}{256} \end{pmatrix}$$

$$\gamma_0 = \frac{5}{256}, \quad \gamma_1 = \frac{15}{64}, \quad \gamma_2 = \frac{63}{128}, \quad \gamma_3 = \frac{15}{64}, \quad \gamma_4 = \frac{5}{256}$$

for $r = 5$.

Similarly,

$$\int_{x_i}^{x_{i+\frac{1}{2}}} p_j(x)dx = \sum_{l=0}^{r-1} b_{jl}\bar{u}_{i+j+l-r+1}, \quad j = 0, \dots, r-1 \quad (2.6)$$

with

$$B = (b_{jl})_{3 \times 3} = \begin{pmatrix} \frac{1}{16} & -\frac{1}{4} & \frac{11}{16} \\ -\frac{1}{16} & \frac{1}{2} & \frac{1}{16} \\ \frac{5}{16} & \frac{1}{4} & -\frac{1}{16} \end{pmatrix}$$

$$\gamma_0 = \frac{3}{16}, \quad \gamma_1 = \frac{5}{8}, \quad \gamma_2 = \frac{3}{16}$$

for $r = 3$, and

$$B = (b_{jl})_{5 \times 5} = \begin{pmatrix} -\frac{7}{256} & \frac{19}{128} & -\frac{11}{32} & \frac{61}{128} & \frac{63}{256} \\ \frac{3}{256} & -\frac{9}{128} & \frac{13}{64} & -\frac{79}{128} & -\frac{7}{256} \\ -\frac{3}{256} & \frac{11}{128} & \frac{1}{2} & \frac{11}{128} & \frac{3}{256} \\ \frac{7}{256} & -\frac{49}{128} & -\frac{13}{64} & \frac{9}{128} & -\frac{3}{256} \\ \frac{256}{193} & \frac{128}{61} & \frac{11}{32} & -\frac{19}{128} & \frac{7}{256} \end{pmatrix}$$

$$\gamma_0 = \frac{5}{256}, \quad \gamma_1 = \frac{15}{64}, \quad \gamma_2 = \frac{63}{128}, \quad \gamma_3 = \frac{15}{64}, \quad \gamma_4 = \frac{5}{256}$$

for $r = 5$.

Notice that the linear weights γ_j are the same for the subintervals $[x_i, x_{i+\frac{1}{2}}]$ and $[x_{i-\frac{1}{2}}, x_i]$. Hence if we use WENO reconstruction to compute one of them and then use the conservation (2.3) to get the other, the result does not depend on which one we choose to compute by WENO.

4. We compute the smoothness indicator, denoted by β_j , for each stencil S_j , which measures how smooth the function $p_j(x)$ is in the target cell I_i . The smaller this smoothness indicator β_j , the smoother the function $p_j(x)$ is in the target cell. In all of the current WENO schemes we use the following smoothness indicator:

$$\beta_j = \sum_{l=1}^{r-1} \int_{I_i} h^{2l-1} \left(\frac{d^l}{dx^l} p_j(x) \right)^2 dx \quad (2.7)$$

Notice that in the actual numerical implementation the smoothness indicators β_j are written out explicitly as quadratic forms of the cell averages of u in the stencil, see [5], [1] and [21] for details.

5. We compute the nonlinear weights based on the smoothness indicators:

$$\omega_j = \frac{\bar{\omega}_j}{\sum_{l=0}^{r-1} \bar{\omega}_l}, \quad \bar{\omega}_j = \frac{\gamma_j}{(\varepsilon + \beta_j)^2} \quad (2.8)$$

where γ_j are the linear weights determined in substep 3 above, and ε is a small number to avoid the denominator to become 0. We use $\varepsilon = 10^{-8}$ in all the computation in this paper. The final WENO approximation is then given by:

$$\frac{1}{h} \int_{x_i}^{x_{i+\frac{1}{2}}} u(x, t^n) dx \approx \sum_{j=0}^{r-1} \omega_j \int_{x_i}^{x_{i+\frac{1}{2}}} p_j(x) dx$$

or

$$\frac{1}{h} \int_{x_{i-\frac{1}{2}}}^{x_i} u(x, t^n) dx \approx \sum_{j=0}^{r-1} \omega_j \int_{x_{i-\frac{1}{2}}}^{x_i} p_j(x) dx.$$

Again, only one of them must be computed because of the conservation property (2.3).

The result does not depend on which one we choose to compute by WENO.

This step produces a reconstruction of $\bar{u}_{i+\frac{1}{2}}^n$ which is $(2r-1)$ -th order accurate. We use $r=3$ and 5 in this paper to obtain fifth and ninth order WENO reconstruction in this step,

respectively. Notice that the WENO stencil in this reconstruction is central. No upwind mechanism is involved.

Step 2. The approximation of $\int_{t^n}^{t^{n+1}} f(u(x_i, t)) dt$. If the time step k is subject to a restrictive CFL condition $k \leq \frac{h}{2} \max |f'(u)|$, we can assume that $u(x_i, t)$ is smooth, since the discontinuities starting at t^n from the staggered grid points $x_{i-\frac{1}{2}}$ and $x_{i+\frac{1}{2}}$ have not reached the cell boundary x_i yet. Hence no Riemann solvers are needed and the time integrals can be evaluated with a quadrature formula to high order accuracy. Notice that this is equivalent to a Lax-Friedrichs scheme and the same effect can also be achieved without a staggered mesh by just using a Lax-Friedrichs building block, such as those WENO finite difference schemes in [5], [1] where the Lax-Friedrichs building blocks are used and no Riemann solvers are needed either. In this paper we use three point Gauss quadrature formula. That is

$$\int_{t^n}^{t^{n+1}} f(u(x_i, t)) dt \approx k \sum_{l=1}^3 \alpha_l f(u(x_i, t^n + k\tau_l))$$

where $\alpha_1 = \alpha_3 = \frac{5}{18}$, $\alpha_2 = \frac{4}{9}$, and $\tau_1 = \frac{1}{2} - \frac{\sqrt{15}}{10}$, $\tau_2 = \frac{1}{2}$, $\tau_3 = \frac{1}{2} + \frac{\sqrt{15}}{10}$ are the weights and knots of the Gauss quadrature formula.

Now what we want to do is to find the approximation of the point values $u(x_i, t^n + k\tau_l)$ from the cell averages $\{\bar{u}_i^n\}$. We consider the conservation laws at the grid points $x = x_i$. At each of these points, the PDE (2.1) reduces to an autonomous ODE in the time variable t .

$$\begin{cases} \frac{du(x_i, t)}{dt} = -(f(u))_x|_{x_i} \\ u(x_i, t^n) \approx u_i^n \end{cases} \quad (2.9)$$

Here u_i^n will be computed by reconstruction from the cell averages $\{\bar{u}_i^n\}$, and the ODE (2.9) will be solved by the classical fourth order Runge-Kutta method to obtain the approximation of $u(x_i, t^n + k\tau_l)$.

This step thus consists of the following substeps:

1. WENO reconstruction of $u_i^n \approx u(x_i, t^n)$. The process of the WENO reconstruction of u_i^n basically follows the substeps 1 to 5 in Step 1 above, with a change in substep 3 to the following:

We find the linear weights, denoted by $\gamma_0, \dots, \gamma_{r-1}$, such that

$$Q(x_i) = \sum_{j=0}^{r-1} \gamma_j p_j(x_i) \quad (2.10)$$

for all possible given data in the stencils. These linear weights depend on the mesh geometry and point x_i , but not on the given solution data in the stencils. Notice that, as before, this substep produces a reconstruction of u_i^n which is $(2r-1)$ -th order accurate. We use $r=3$ and 5 again to obtain fifth and ninth order WENO reconstruction in this substep, respectively. The WENO stencil in this reconstruction is again central. No upwind mechanism is involved. The polynomials $p_j(x)$ involved here are the same as the ones in the first step above to reconstruct $\bar{u}_{i+\frac{1}{2}}^n$, hence the smoothness indicators (2.7) do not need to be re-computed.

For example, when $r=3$ and 5 , we have

$$p_j(x_i) = \sum_{l=0}^{r-1} c_{jl} \bar{u}_{i+j+l-r+1}, \quad j = 0, \dots, r-1 \quad (2.11)$$

with

$$C = (c_{jl})_{3 \times 3} = \begin{pmatrix} -\frac{1}{24} & \frac{1}{12} & \frac{23}{24} \\ \frac{1}{24} & \frac{1}{12} & -\frac{1}{24} \\ \frac{23}{24} & \frac{1}{12} & -\frac{1}{24} \end{pmatrix}$$

$$\gamma_0 = -\frac{9}{80}, \quad \gamma_1 = \frac{49}{40}, \quad \gamma_2 = -\frac{9}{80}$$

for $r = 3$, and

$$C = (c_{jl})_{5 \times 5} = \begin{pmatrix} -\frac{71}{1920} & \frac{91}{480} & -\frac{373}{960} & \frac{57}{160} & \frac{563}{640} \\ \frac{640}{3} & -\frac{160}{3} & -\frac{13}{960} & \frac{511}{480} & -\frac{71}{1920} \\ \frac{640}{3} & -\frac{29}{29} & \frac{1067}{960} & -\frac{29}{480} & \frac{3}{1920} \\ \frac{640}{71} & \frac{480}{511} & \frac{960}{13} & -\frac{480}{3} & \frac{640}{3} \\ -\frac{1920}{563} & \frac{480}{57} & -\frac{960}{373} & -\frac{160}{91} & \frac{640}{71} \\ \frac{640}{640} & \frac{160}{160} & -\frac{960}{960} & \frac{480}{480} & -\frac{71}{1920} \end{pmatrix}$$

$$\gamma_0 = -\frac{525}{163584}, \quad \gamma_1 = -\frac{63425}{286272}, \quad \gamma_2 = \frac{11689}{8064}, \quad \gamma_3 = -\frac{63425}{286272}, \quad \gamma_4 = -\frac{525}{163584}$$

for $r = 5$.

We remark that it is easy to verify that, when r is an even number ($r=2, 4, \dots$), there are no linear weights that satisfy condition (2.10). Hence there are no third, seventh,

eleventh, etc. order central WENO reconstructions for the point values u_i^n with these choices of stencils.

From (2.11) we notice that two of linear weights are negative. When linear weights become negative, the usual WENO approximation is unstable. Here we adopt the splitting technique of treating negative weights in WENO schemes developed by Shi, Hu and Shu [19]: we first split the linear weights into two groups

$$\tilde{\gamma}_i^+ = \frac{1}{2}(\gamma_i + 3|\gamma_i|), \quad \tilde{\gamma}_i^- = \tilde{\gamma}_i^+ - \gamma_i, \quad i = 0, \dots, r-1$$

and scale them by

$$\sigma^\pm = \sum_{j=0}^{r-1} \tilde{\gamma}_j^\pm; \quad \gamma_i^\pm = \tilde{\gamma}_i^\pm / \sigma^\pm, \quad i = 1, \dots, r-1.$$

For example, when $r=3$, we obtain

$$\tilde{\gamma}_0^+ = \frac{9}{80}, \quad \tilde{\gamma}_1^+ = \frac{49}{20}, \quad \tilde{\gamma}_2^+ = \frac{9}{80}; \quad \tilde{\gamma}_0^- = \frac{9}{40}, \quad \tilde{\gamma}_1^- = \frac{49}{40}, \quad \tilde{\gamma}_2^- = \frac{9}{40},$$

and

$$\sigma^+ = \frac{107}{40}, \quad \sigma^- = \frac{67}{40};$$

$$\gamma_0^+ = \frac{9}{214}, \quad \gamma_1^+ = \frac{98}{107}, \quad \gamma_2^+ = \frac{9}{214}; \quad \gamma_0^- = \frac{9}{67}, \quad \gamma_1^- = \frac{49}{67}, \quad \gamma_2^- = \frac{9}{67}.$$

The WENO reconstruction is now performed on each group separately, by computing the nonlinear weights (2.8) separately for ω_j^\pm with the same smoothness indicators β_j in (2.7). The final WENO reconstruction is then taken as σ^+ times the reconstruction using the group of positive weights minus σ^- times the reconstruction using the group of negative weights. The key idea of this decomposition is to make sure that every stencil has a significant representation in both the positive and the negative weight groups. Within each group, the WENO idea of redistributing the weights subject to a fixed sum according to the smoothness of the approximation is still followed as before. For more details, we refer to [19].

2. The Runge-Kutta method with the aid of natural continuous extension (NCE) for (2.9). If the classical fourth order Runge-Kutta method is used to compute each of the $u(x_i, t^n + k\tau_l)$ to fourth order accuracy, we would need to reconstruct f_x four times for each $u(x_i, t^n + k\tau_l)$. This would become extremely costly. Bianco et al. [2] initialized a strategy to achieve a significant saving in computational cost by using the NCE of a Runge-Kutta scheme developed by Zennaro [24]. This is the strategy we will also use in this paper.

For simplicity we shall only describe the fourth order NCE Runge-Kutta method which will be used in this paper. Further details about NCE can be found in [2, 24]. Consider the Cauchy problem:

$$\begin{cases} y'(t) = F(t, y(t)) \\ y(t_0) = y_0 \end{cases} \quad (2.12)$$

Then the solution at the $(n+1)$ -th time step obtained with the traditional fourth order Runge-Kutta scheme can be written as:

$$y^{n+1} = y^n + k \sum_{j=1}^4 b_j g^{(j)}$$

where $b_1 = b_4 = \frac{1}{6}$, $b_2 = b_3 = \frac{1}{3}$ and the $g^{(j)}$ are the approximate Runge-Kutta fluxes

$$\begin{aligned} g^{(1)} &= F(t^n, y^n) \\ g^{(2)} &= F(t^n + c_2 k, y^n + \frac{k}{2} g^{(1)}) \\ g^{(3)} &= F(t^n + c_3 k, y^n + \frac{k}{2} g^{(2)}) \\ g^{(4)} &= F(t^n + c_4 k, y^n + k g^{(3)}) \\ c_2 = c_3 &= \frac{1}{2}, c_4 = 1 \end{aligned}$$

For this Runge-Kutta scheme there exist four third order polynomials

$$\begin{aligned} b_1(\theta) &= 2(1 - 4b_1)\theta^3 + 3(3b_1 - 1)\theta^2 + \theta, \\ b_j(\theta) &= 4(3c_j - 2)b_j\theta^3 + 3(3 - 4c_j)b_j\theta^2, \quad j = 2, 3, 4 \end{aligned}$$

such that the natural continuous extension z of degree 3 satisfies:

$$\begin{aligned} z(t^n + \theta k) &:= y^n + k \sum_{j=1}^4 b_j(\theta) g^{(j)}, \quad 0 \leq \theta \leq 1; \\ z(t^n) &= y^n \quad \text{and} \quad z(t^{n+1}) = y^{n+1}; \\ \max_{t^n \leq t \leq t^{n+k}} |y^{(l)}(t) - z^{(l)}(t)| &= O(k^{4-l}), \quad 0 \leq l \leq 4 \end{aligned}$$

where $y(t)$ is the exact solution of (2.12) with $y(t^n) = y^n$.

Thus at each time step, we apply the Runge-Kutta scheme only once, and obtain all intermediate values $u(x_i, t^n + k\tau_l)$ to fourth order accuracy through the evaluation of the NCE.

3. WENO approximation of $f(u)_x|_{x=x_i}$ from $\{u_i = u(x_i, t)\}$. We denote $f_i = f(u_i)$. This substep consists of the following sub-substeps:

- (a) We identify several point sets $S_j, j = 0, \dots, r-1$, such that x_i belongs to each of them. Here we set $S_j = \cup_{l=0}^{r-1} x_{i+j-l}$. We denote by $\mathcal{T} = \cup_{j=0}^{r-1} S_j$ the larger set which contains all the points from the r smaller sets.
- (b) We have a $(r-1)$ -th degree interpolating polynomial function denoted by $p_j(x)$, associated with each of the sets $S_j, j = 0, \dots, r-1$, such that $p_j(x_{i+j-l}) = f_{i+j-l}, l = 0, \dots, r-1$. We also have a higher $(2r-2)$ -th degree interpolating polynomial function denoted by $Q(x)$, associated with the larger set \mathcal{T} , such that $Q(x_{i+l}) = f_{i+l}, l = -r+1, \dots, r-1$.
- (c) We find the linear weights, denoted by $\gamma_0, \dots, \gamma_{r-1}$, such that

$$Q'(x_i) = \sum_{j=0}^{r-1} \gamma_j p_j'(x_i) \quad (2.13)$$

for all possible given data in the set. These linear weights depend on the mesh geometry and the point x_i , but not on the given solution data in the set.

In this paper we set $r=3$ and 5 for the fourth and eighth order accurate approximation to the derivative $f(u)_x|_{x=x_i}$, respectively. This is the place where the order is lowered by one. The two previous reconstructions, from $\{\bar{u}_i^n\}$ to $\{\bar{u}_{i+\frac{1}{2}}^n\}$ and from $\{\bar{u}_i^n\}$ to $\{u_i^n\}$, are both fifth and ninth order accurate, respectively, for $r=3$ and 5 . This is due to the fact that the approximation to the derivative is one order lower than that to the function itself when the same stencil is used. We also notice that this approximation to $f(u)_x|_{x=x_i}$ is purely central. No upwind mechanism is present. To make up for this loss of one order of accuracy, and

also to introduce some upwinding mechanism (artificial viscosity at the level of truncation error), we could perform a Lax-Friedrich flux splitting:

$$f^\pm(u) = \frac{1}{2}(f(u) \pm \alpha u), \quad \alpha = \max_u |f'(u)|$$

where the maximum is taken over u_i^n for all i . We could then use one more grid point, added either to the left for $f^+(u)$ or to the right for $f^-(u)$, in the approximation to the derivatives $f^\pm(u)_{x|x=x_i}$, thus getting fifth and ninth order accurate approximations.

For example, when $r=3$ and 5, we have

$$p'_j(x_i) = \sum_{l=0}^{r-1} d_{jl} f_{i+j+l-r+1}, \quad j = 0, \dots, r-1 \quad (2.14)$$

with

$$D = (d_{jl})_{3 \times 3} = \begin{pmatrix} \frac{1}{2} & -2 & \frac{3}{2} \\ -\frac{1}{2} & 0 & \frac{1}{2} \\ -\frac{3}{2} & 2 & -\frac{1}{2} \end{pmatrix}$$

$$\gamma_0 = \frac{1}{6}, \quad \gamma_1 = \frac{2}{3}, \quad \gamma_2 = \frac{1}{6}$$

for $r = 3$, and

$$D = (d_{jl})_{5 \times 5} = \begin{pmatrix} \frac{1}{4} & -\frac{4}{3} & 3 & -4 & \frac{25}{12} \\ -\frac{1}{12} & \frac{1}{2} & -\frac{3}{2} & \frac{5}{6} & \frac{1}{4} \\ \frac{1}{12} & -\frac{2}{3} & 0 & \frac{2}{3} & -\frac{1}{12} \\ -\frac{1}{4} & \frac{5}{6} & \frac{3}{2} & -\frac{1}{2} & \frac{1}{12} \\ -\frac{25}{12} & 4 & -3 & \frac{4}{3} & \frac{1}{4} \end{pmatrix}$$

$$\gamma_0 = \frac{1}{70}, \quad \gamma_1 = \frac{8}{35}, \quad \gamma_2 = \frac{18}{35}, \quad \gamma_3 = \frac{8}{35}, \quad \gamma_4 = \frac{1}{70}$$

for $r = 5$.

If flux splitting is used and one more grid point is added, then we have

$$p'_j(x_i) = \sum_{l=0}^r d_{jl}^- f_{i+j+l-r+1}^-, \quad j = 0, \dots, r-1 \quad (2.15)$$

for $f^-(u)$, with

$$D^- = (d_{jl}^-)_{3 \times 4} = \begin{pmatrix} \frac{1}{6} & -1 & \frac{1}{2} & \frac{1}{3} \\ -\frac{1}{3} & -\frac{1}{2} & 1 & -\frac{1}{6} \\ -\frac{11}{6} & 3 & -\frac{3}{2} & \frac{1}{3} \end{pmatrix}$$

$$\gamma_0 = \frac{3}{10}, \quad \gamma_1 = \frac{3}{5}, \quad \gamma_2 = \frac{1}{10}$$

for $r = 3$, and

$$D^- = (d_{jl}^-)_{5 \times 6} = \begin{pmatrix} \frac{1}{20} & -\frac{1}{3} & 1 & -2 & \frac{13}{12} & \frac{1}{5} \\ -\frac{1}{30} & \frac{1}{4} & -1 & \frac{1}{3} & \frac{1}{2} & -\frac{1}{20} \\ \frac{1}{20} & -\frac{1}{2} & -\frac{1}{3} & 1 & -\frac{1}{4} & \frac{1}{30} \\ -\frac{1}{5} & -\frac{13}{12} & 2 & -1 & \frac{1}{3} & -\frac{1}{20} \\ -\frac{13}{60} & 5 & -5 & \frac{10}{3} & -\frac{5}{4} & \frac{1}{5} \end{pmatrix}$$

$$\gamma_0 = \frac{1}{126}, \quad \gamma_1 = \frac{10}{63}, \quad \gamma_2 = \frac{10}{21}, \quad \gamma_3 = \frac{20}{63}, \quad \gamma_4 = \frac{5}{126}$$

for $r = 5$. The approximation for $f^+(u)$ is mirror symmetric with respect to x_i .

- (d) Compute the smoothness indicators, denoted by β_j . We still use the same smoothness indicators as before:

$$\beta_j = \sum_{l=1}^{r-1} \int_{I_i} h^{2l-1} \left(\frac{d^l}{dx^l} p_j(x) \right)^2 dx \quad (2.16)$$

We can write these smoothness indicators β_j out explicitly as quadratic forms of f_i in the stencil.

- (e) As before, we compute the nonlinear weights based on the smoothness indicators:

$$\omega_j = \frac{\bar{\omega}_j}{\sum_{l=0}^{r-1} \bar{\omega}_l}, \quad \bar{\omega}_j = \frac{\gamma_j}{(\varepsilon + \beta_j)^2} \quad (2.17)$$

where γ_j are the linear weights determined in sub-substep (c) above, and ε is a small number to avoid the denominator to become 0. As before, we use $\varepsilon = 10^{-8}$ here in all the computation. The final WENO approximation is then given by:

$$f(u)_x|_{x=x_i} \approx \sum_{j=0}^{r-1} \omega_j p'_j(x_i) \quad (2.18)$$

Following the above steps we can evolve the numerical solution from a time step to the next time step on a staggered mesh, and in the following time step we repeat the solution process and come back to the original mesh.

We remark that there are three WENO reconstruction or approximation steps at time level t^n , namely the WENO reconstruction from $\{\bar{u}_i^n\}$ to $\{\bar{u}_{i+\frac{1}{2}}^n\}$, the WENO reconstruction

from $\{\bar{u}_i^n\}$ to $\{u_i^n\}$, and the WENO approximation from $\{u_i^n\}$ to $\{f(u)_x|_{x=x_i}\}$. However, the first two reconstructions share the same smoothness indicators, which is one of the most costly parts of the procedure. For each additional Runge-Kutta inner stage (there are three additional inner stages for the fourth order Runge-Kutta method), only one WENO approximation from $\{u_i\}$ to $\{f(u)_x|_{x=x_i}\}$ is needed. This should be compared with a non-staggered finite difference WENO scheme in [5] and [1] where only one WENO reconstruction is needed per Runge-Kutta inner stage, including the first one at time level t^n .

For systems of conservation laws, such as the Euler equations of gas dynamics, all three WENO reconstructions and approximations (from $\{\bar{u}_i^n\}$ to $\{\bar{u}_{i+\frac{1}{2}}^n\}$, from $\{\bar{u}_i^n\}$ to $\{u_i^n\}$, and from $\{u_i^n\}$ to $\{f(u)_x|_{x=x_i}\}$) could either be performed in each component or in local characteristic directions. The local characteristic decomposition certainly increases the computational cost. It is usually noted in the literature that such local characteristic decomposition is unnecessary for central schemes. In fact this is also true for some non-central schemes, e.g. [13]. However, most of such schemes are second order, or at most third order accurate. In the following section of numerical experiments we will explore when and where it is necessary to perform such local characteristic decompositions when the order of accuracy is higher.

3 Numerical results

In this section we provide numerical experiment results for the fourth and eighth order CWENO schemes developed in the previous section, as well as compare them with the finite difference WENO schemes in [5] and [1]. The CFL number is taken as 0.4 in all the numerical tests.

3.1 Accuracy test

We first test the accuracy of the schemes on linear scalar problems, nonlinear scalar problems and nonlinear systems.

Table 3.1: $u_t + u_x = 0$. $u(x, 0) = \sin(\pi x)$. CWENO-4 with periodic boundary conditions. $t = 10$. L^1 and L^∞ errors. Uniform meshes with N grid points.

N	L_1 error	L_1 order	L_∞ error	L_∞ order
10	4.31426E-01		3.27349E-01	
20	2.59113E-02	4.05746	1.79819E-02	4.18621
40	9.24181E-04	4.80926	7.21317E-04	4.63977
80	2.86307E-05	5.01254	2.49636E-05	4.85274
160	8.93602E-07	5.00179	7.97193E-07	4.96875
320	2.78747E-08	5.00260	2.54104E-08	4.97144
640	8.65318E-10	5.00958	7.51897E-10	5.07874
1280	2.63427E-11	5.03776	2.26752E-11	5.05135

Example 3.1. We solve the following linear scalar problem

$$u_t + u_x = 0 \tag{3.1}$$

with two different initial conditions, $u(x, 0) = \sin(\pi x)$ and $u(x, 0) = \sin^4(\pi x)$, with 2-periodic boundary conditions. The second initial condition is typically more difficult to ENO type schemes to achieve full order of accuracy [20]. We compute the solution up to $t = 10$, i.e. after 5 time periods. The results are shown in Tables 3.1-3.4. We can see that both the fourth order central WENO (CWENO-4) and the eighth order central WENO (CWENO-8) achieve or exceed their designed order of accuracy for both initial conditions.

Example 3.2. We solve the following nonlinear scalar Burgers equation

$$u_t + \left(\frac{u^2}{2}\right)_x = 0 \tag{3.2}$$

with the initial condition $u(x, 0) = 0.5 + \sin(\pi x)$, with 2-periodic boundary conditions. When $t = 0.5/\pi$ the solution is still smooth, and the errors and numerical orders of accuracy are shown in Tables 3.5-3.6. We can see that both the fourth order central WENO (CWENO-4) and the eighth order central WENO (CWENO-8) achieve or exceed their designed order of accuracy.

Table 3.2: $u_t + u_x = 0$. $u(x, 0) = \sin^4(\pi x)$. CWENO-4 with periodic boundary conditions. $t = 10$. L^1 and L^∞ errors. Uniform meshes with N grid points.

N	L_1 error	L_1 order	L_∞ error	L_∞ order
10	6.76623E-01		4.53698E-01	
20	2.09760E-01	1.68961	2.42694E-01	0.90259
40	3.81273E-02	2.45985	3.99979E-02	2.60114
80	4.04333E-03	3.23721	8.55933E-03	2.22435
160	2.71260E-04	3.89779	1.32746E-03	2.68883
320	6.89724E-06	5.29751	4.19959E-05	4.98228
640	1.40480E-07	5.61758	7.72119E-07	5.76528
1280	3.46085E-09	5.34310	1.32125E-08	5.86884

Table 3.3: $u_t + u_x = 0$. $u(x, 0) = \sin(\pi x)$. CWENO-8 with periodic boundary conditions. $t = 10$. L^1 and L^∞ errors. Uniform meshes with N grid points.

N	L_1 error	L_1 order	L_∞ error	L_∞ order
10	3.30104E-03		2.52900E-03	
20	2.22664E-05	7.21191	2.05075E-05	6.94627
40	5.47689E-08	8.66730	6.16808E-08	8.37712
80	2.47113E-10	7.79204	2.14888E-10	8.16509

Table 3.4: $u_t + u_x = 0$. $u(x, 0) = \sin^4(\pi x)$. CWENO-8 with periodic boundary conditions. $t = 10$. L^1 and L^∞ errors. Uniform meshes with N grid points.

N	L_1 error	L_1 order	L_∞ error	L_∞ order
10	6.08172E-01		3.93953E-01	
20	1.39739E-01	2.12174	1.36330E-01	1.53092
40	3.98223E-03	5.13302	6.76581E-03	4.33269
80	6.05187E-05	6.04005	2.02169E-04	5.06463
160	9.23852E-08	9.35550	3.96918E-07	8.99251
320	4.12995E-10	7.80539	1.75471E-09	7.82147

Table 3.5: $u_t + \left(\frac{u^2}{2}\right)_x = 0$. $u(x, 0) = 0.5 + \sin(\pi x)$. CWENO-4 with periodic boundary conditions. $t = 0.5/\pi$. L^1 and L^∞ errors. Uniform meshes with N grid points.

N	L_1 error	L_1 order	L_∞ error	L_∞ order
10	2.18015E-02		4.02010E-02	
20	4.10383E-03	2.40939	1.10126E-02	1.86807
40	1.30736E-04	4.97224	6.70316E-04	4.03818
80	3.86494E-06	5.08007	2.56052E-05	4.71033
160	1.12062E-07	5.10808	7.76128E-07	5.04400
320	3.18798E-09	5.13551	2.21469E-08	5.13112
640	9.44782E-11	5.07652	6.48043E-10	5.09487
1280	2.76844E-12	5.09284	1.82380E-11	5.15107

Table 3.6: $u_t + \left(\frac{u^2}{2}\right)_x = 0$. $u(x, 0) = 0.5 + \sin(\pi x)$. CWENO-8 with periodic boundary conditions. $t = 0.5/\pi$. L^1 and L^∞ errors. Uniform meshes with N grid points.

N	L_1 error	L_1 order	L_∞ error	L_∞ order
10	2.99436E-02		6.09818E-02	
20	2.06968E-03	3.85477	6.93168E-03	3.13710
40	5.11460E-05	5.33864	2.67653E-04	4.69477
80	4.48201E-07	6.83433	3.76899E-06	6.15004
160	1.73253E-09	8.01512	1.69149E-08	7.79974
320	5.18318E-12	8.38483	5.36330E-11	8.30096

Example 3.3. We solve the following nonlinear system of Euler equations

$$u_t + f(u)_x = 0 \tag{3.3}$$

with

$$u = (\rho, \rho v, E)^T, \quad f(u) = (\rho v, \rho v^2 + p, v(E + p))^T,$$

Here ρ is the density, v is the velocity, E is the total energy, p is the pressure, related to the total energy by $E = \frac{p}{\gamma-1} + \frac{1}{2}\rho v^2$ with $\gamma = 1.4$. The initial condition is set to be $\rho(x, 0) = 1 + 0.2 \sin(\pi x)$, $v(x, 0) = 1$, $p(x, 0) = 1$, with 2-periodic boundary conditions. The exact solution is $\rho(x, t) = 1 + 0.2 \sin(\pi(x - t))$, $v = 1$, $p = 1$. We compute the solution up to $t = 2$ using componentwise WENO reconstructions and various characteristic and flux splitting WENO reconstructions outlined at the end of the last section, i.e. we perform one, two, or three out of the three WENO reconstructions and approximations (from $\{\bar{u}_i^n\}$ to $\{\bar{u}_{i+\frac{1}{2}}^n\}$, from $\{\bar{u}_i^n\}$ to $\{u_i^n\}$, and from $\{u_i^n\}$ to $\{f(u)_x|_{x=x_i}\}$) in local characteristic directions and the remaining componentwise. For this smooth test case, all cases produce similar errors and orders of accuracy. The errors and numerical orders of accuracy of the density ρ for the componentwise WENO reconstructions are shown in Tables 3.7-3.8. We can see that both the fourth order central WENO (CWENO-4) and the eighth order central WENO (CWENO-8) achieve or exceed their designed order of accuracy.

3.2 Test cases with shocks

Example 3.4. We solve the same nonlinear Burgers equation (3.2) as in Example 3.2 with the same initial condition $u(x, 0) = 0.5 + \sin(\pi x)$, except that we now plot the results at $t = 1.5/\pi$ when a shock has already appeared in the solution. In Figure 3.1, the solutions of CWENO-4 (left) and CWENO-8 (right) with $N = 80$ grid points are shown. The solid line is the exact solution. We can see that both schemes give non-oscillatory shock transitions for this problem.

Table 3.7: Euler equations. $\rho(x, 0) = 1 + 0.2 \sin(\pi x)$, $v(x, 0) = 1$, $p(x, 0) = 1$. CWENO-4 with periodic boundary conditions. $t = 2$. L^1 and L^∞ errors of density ρ . Uniform meshes with N grid points.

N	L_1 error	L_1 order	L_∞ error	L_∞ order
20	1.78676E-03		1.49231E-03	
40	1.03208E-04	4.11372	1.13337E-04	3.71885
80	6.46312E-06	3.99718	1.04821E-05	3.43463
160	1.00454E-07	6.00762	1.62502E-07	6.01132
320	1.18655E-09	6.40362	1.29325E-09	6.97331
640	3.81902E-11	4.95743	3.64027E-11	5.15081
1280	1.18452E-12	5.01083	1.06781E-12	5.09131

Table 3.8: Euler equations. $\rho(x, 0) = 1 + 0.2 \sin(\pi x)$, $v(x, 0) = 1$, $p(x, 0) = 1$. CWENO-8 with periodic boundary conditions. $t = 2$. L^1 and L^∞ errors of density ρ . Uniform meshes with N grid points.

N	L_1 error	L_1 order	L_∞ error	L_∞ order
10	6.47260E-05		5.00036E-05	
20	2.01132E-07	8.33006	1.59030E-07	8.29659
40	5.74818E-10	8.45082	4.51485E-10	8.46040
80	1.62601E-12	8.46562	1.28186E-12	8.46029

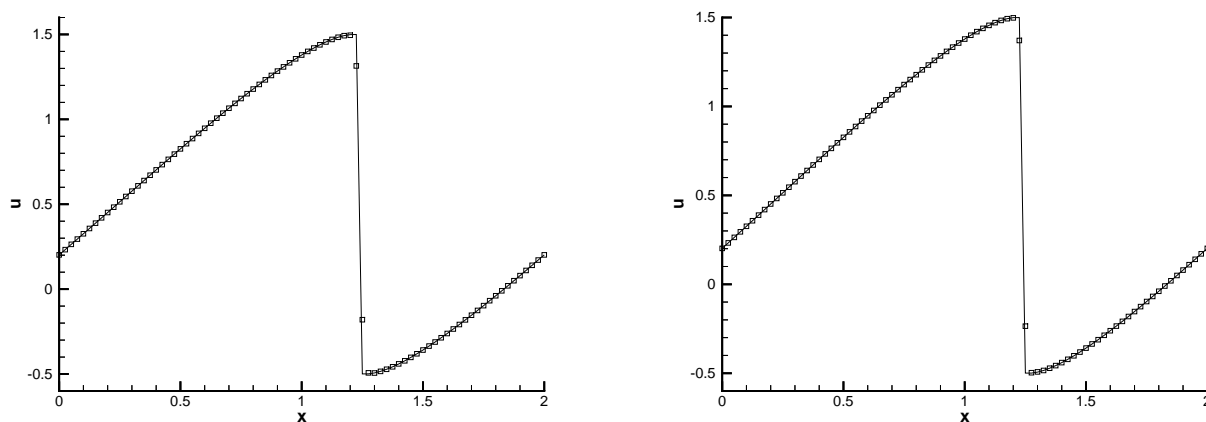


Figure 3.1: Burgers equation. $u(x, 0) = 0.5 + \sin(\pi x)$. $t = 1.5/\pi$. $N = 80$ points. Left: CWENO-4; right: CWENO-8. Solid line: exact solution; squares: computed solution.

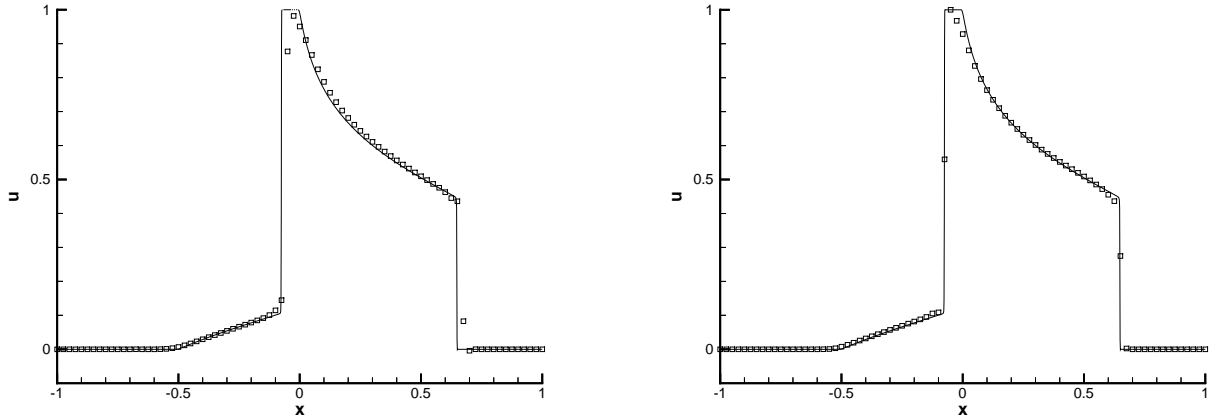


Figure 3.2: The Buckley-Leverett problem. $t = 0.4$. $N = 81$ points. Left: CWENO-4; right: CWENO-8. Solid line: exact solution; squares: computed solution.

Example 3.5. We solve the nonlinear non-convex scalar Buckley-Leverett problem

$$u_t + \left(\frac{4u^2}{4u^2 + (1-u)^2} \right)_x = 0 \quad (3.4)$$

with the initial data $u = 1$ when $-\frac{1}{2} \leq x \leq 0$ and $u = 0$ elsewhere. The solution is computed up to $t = 0.4$. The exact solution is a shock-rarefaction-contact discontinuity mixture. We remark that some high order schemes may fail to converge to the correct entropy solution for this problem. In Figure 3.2, the solutions of CWENO-4 (left) and CWENO-8 (right) with $N = 81$ grid points are shown. The solid line is the exact solution. We can see that both schemes give good resolutions to the correct entropy solution for this problem.

Example 3.6. We solve the same Euler equations (3.3) but now with a Riemann initial condition for the Lax Problem:

$$(\rho, v, p) = (0.445, 0.698, 3.528) \text{ for } x \leq 0; \quad (\rho, v, p) = (0.5, 0, 0.571) \text{ for } x > 0.$$

The computed density ρ is plotted at $t = 0.16$ against the exact solution. In Figure 3.3 we plot the solution with CWENO-4 using componentwise WENO reconstruction, with $N = 200$ grid points (left) and $N = 400$ grid points (right). We can see that the results are oscillatory but the oscillations become less significant when the mesh is refined. For a comparison,

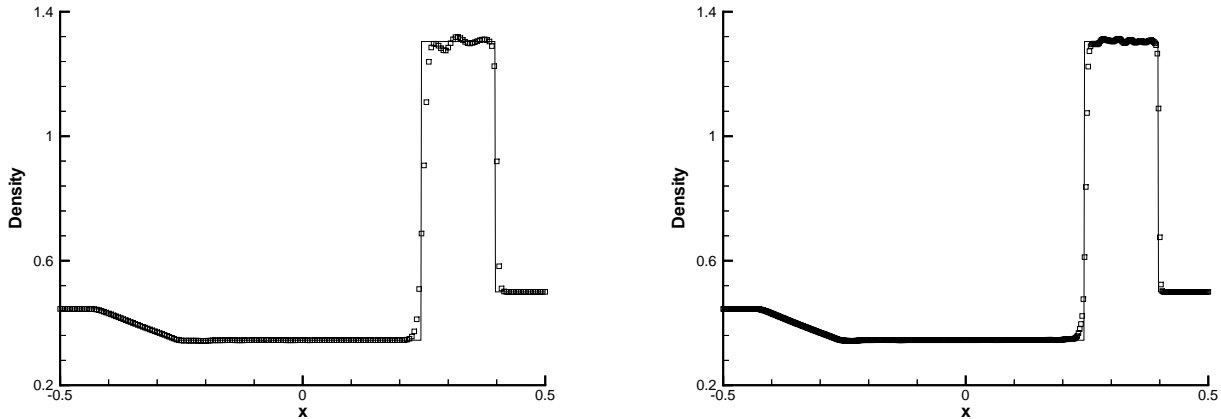


Figure 3.3: The Lax problem. $t = 0.16$. CWENO-4 scheme with componentwise WENO reconstructions. Left: $N = 200$ grid points; right: $N = 400$ grid points. Solid line: exact solution; squares: computed solution.

In Figure 3.4 we plot the solution with the finite difference fifth order WENO scheme on a non-staggered mesh in [5] using componentwise reconstructions, also with $N = 200$ grid points (left) and $N = 400$ grid points (right). We can see that these are also oscillatory and the oscillations are a bit more serious than for the central CWENO-4 scheme.

We repeat the experiment for the CWENO-8 schemes using componentwise WENO reconstructions in Figure 3.5, and for the ninth order finite difference WENO scheme on a non-staggered mesh in [1] in Figure 3.6. We can see that the oscillations become more serious when the order of accuracy is increased. Also, as before, the non-staggered WENO scheme has more serious oscillations than the central CWENO-8 scheme.

We have also experimented with using a single quantity (e.g. density ρ) for computing the smoothness indicator for all components. The results are similarly oscillatory.

We conclude from this example that componentwise WENO will become more oscillatory when the order of accuracy increases, both for the central WENO schemes and for the usual finite difference WENO schemes on a non-staggered mesh, although the central WENO with a staggered mesh tends to give smaller oscillations.

We demonstrate that a local characteristic decomposition in the WENO reconstruction

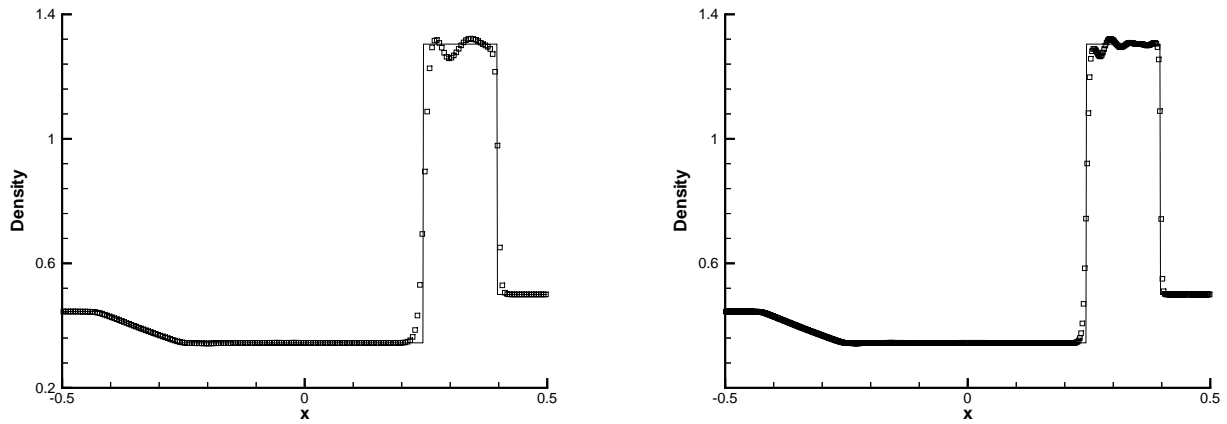


Figure 3.4: The Lax problem. $t = 0.16$. WENO-5 finite difference scheme [5] with componentwise reconstruction. Left: $N = 200$ grid points; right: $N = 400$ grid points. Solid line: exact solution; squares: computed solution.

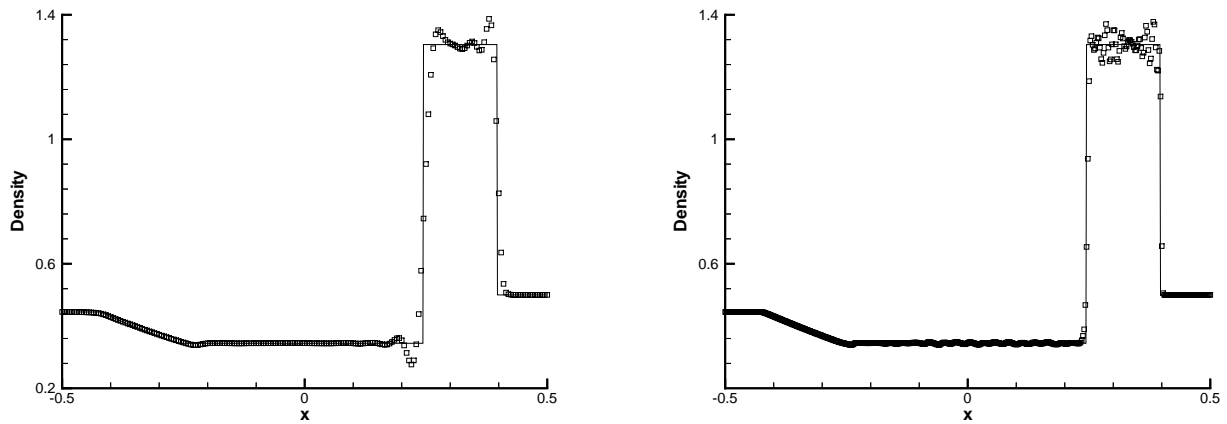


Figure 3.5: The Lax problem. $t = 0.16$. CWENO-8 scheme with componentwise WENO reconstructions. Left: $N = 200$ grid points; right: $N = 400$ grid points. Solid line: exact solution; squares: computed solution.

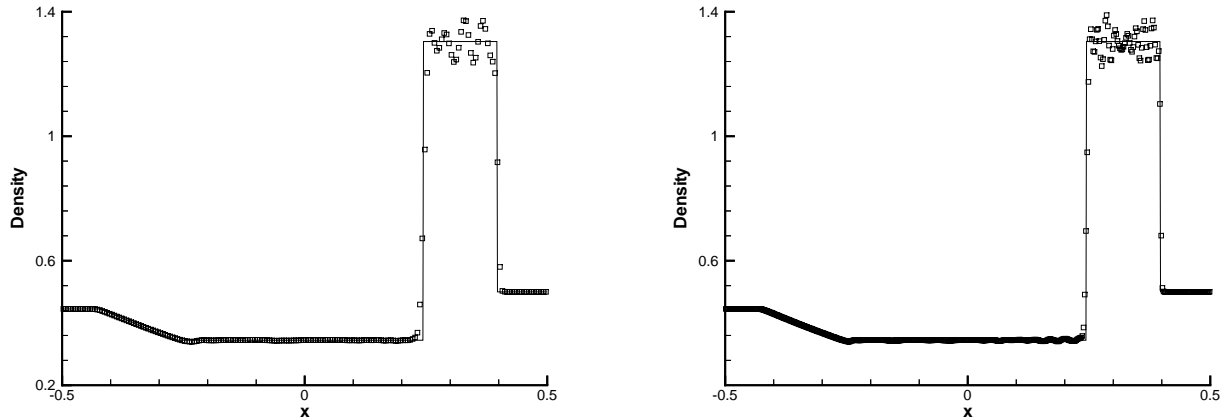


Figure 3.6: The Lax problem. $t = 0.16$. WENO-9 finite difference scheme [1] with componentwise reconstruction. Left: $N = 200$ grid points; right: $N = 400$ grid points. Solid line: exact solution; squares: computed solution.

procedure effectively removes the oscillations. In fact, we have found out after extensive numerical experiments that, as long as one does the local characteristic decomposition for the reconstruction from $\{\bar{u}_i^n\}$ to $\{\bar{u}_{i+\frac{1}{2}}^n\}$, one can still use componentwise WENO reconstruction from $\{\bar{u}_i^n\}$ to $\{u_i^n\}$ and componentwise WENO approximation from $\{u_i^n\}$ to $\{f(u)_x|_{x=x_i}\}$ and effectively remove all the spurious oscillations. See Figure 3.7 for the results of the CWENO-4 scheme and Figure 3.9 for the results of the CWENO-8 scheme. For comparison, we plot the results of the fifth order finite difference WENO scheme using local characteristic decompositions on a non-staggered mesh [5] in Figure 3.8, and the ninth order finite difference WENO scheme using local characteristic decompositions on a non-staggered mesh [1] in Figure 3.10. We can see that when local characteristic decomposition is used, both the central WENO schemes based on staggered mesh and the finite difference WENO schemes based on non-staggered mesh give beautiful non-oscillatory results.

Example 3.7. The previous examples contain only shocks and simple smooth region solutions (almost piecewise linear), for which shock resolution is the main concern and usually a good second order non-oscillatory scheme would give satisfactory results. There is little advantage in using higher order schemes for such cases. We have been using them in the nu-

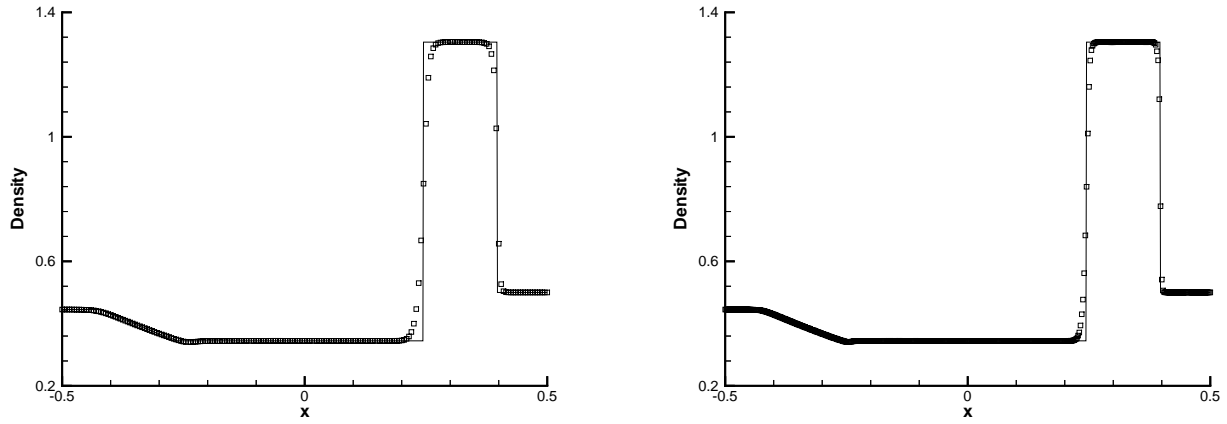


Figure 3.7: The Lax problem. $t = 0.16$. CWENO-4 scheme with local characteristic decomposition for the WENO reconstruction of $\bar{u}_{j+\frac{1}{2}}$. Left: $N = 200$ grid points; right: $N = 400$ grid points. Solid line: exact solution; squares: computed solution.

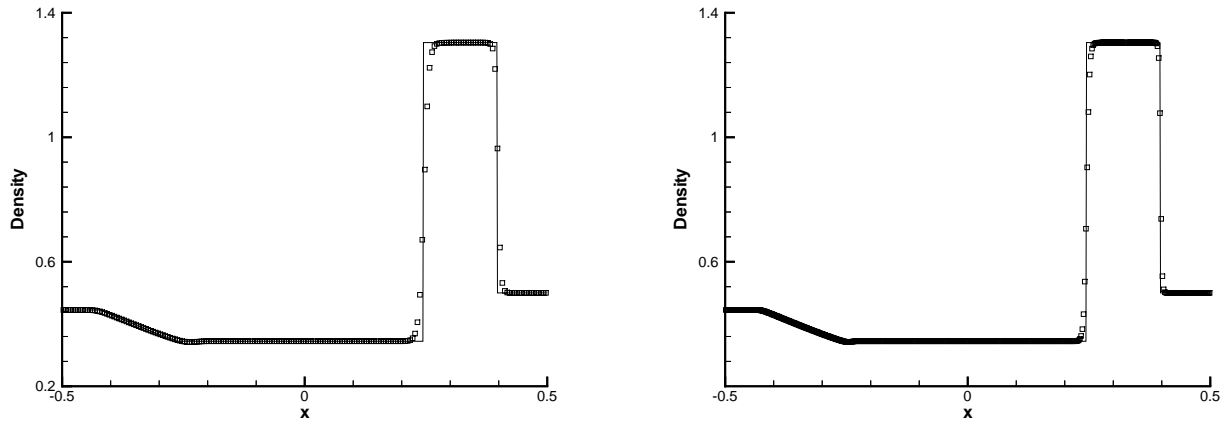


Figure 3.8: The Lax problem. $t = 0.16$. WENO-5 finite difference scheme [5] with local characteristic decomposition. Left: $N = 200$ grid points; right: $N = 400$ grid points. Solid line: exact solution; squares: computed solution.

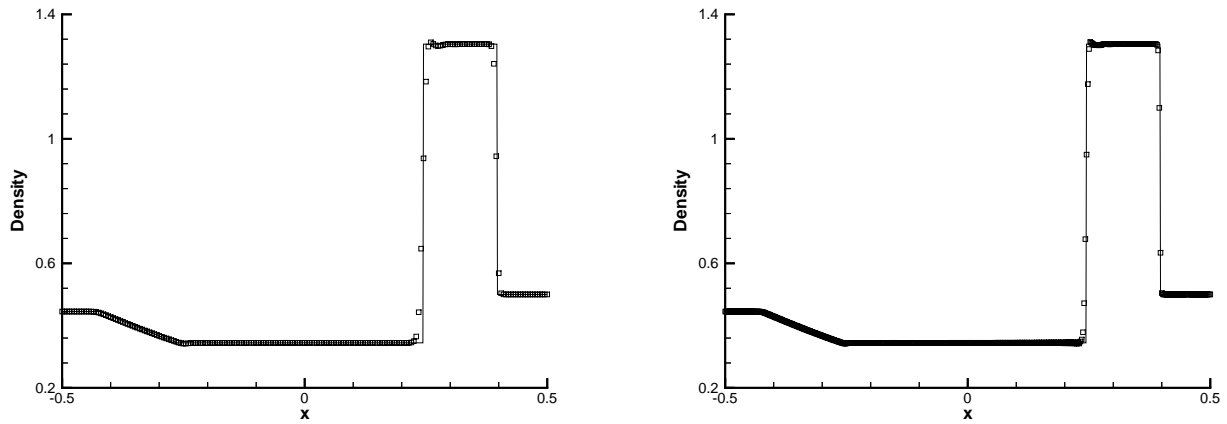


Figure 3.9: The Lax problem. $t = 0.16$. CWENO-8 scheme with local characteristic decomposition for the WENO reconstruction of $\bar{u}_{j+\frac{1}{2}}$. Left: $N = 200$ grid points; right: $N = 400$ grid points. Solid line: exact solution; squares: computed solution.

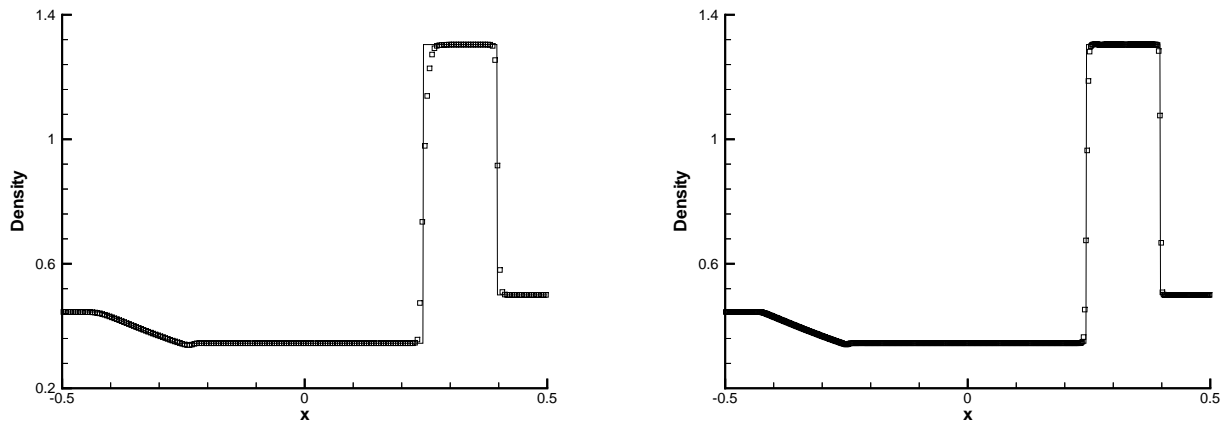


Figure 3.10: The Lax problem. $t = 0.16$. WENO-9 finite difference scheme [1] with local characteristic decomposition. Left: $N = 200$ grid points; right: $N = 400$ grid points. Solid line: exact solution; squares: computed solution.

merical experiments mainly to demonstrate the non-oscillatory properties of the high order schemes. A higher order scheme would show its advantage when the solution contains both shocks and complex smooth region structures. A typical example for this is the problem of shock interaction with entropy waves [23]. We solve the same Euler equations (3.3) with a moving Mach=3 shock interacting with sine waves in density, i.e. initially

$$(\rho, v, p) = (3.857143, 2.629369, 10.333333) \text{ for } x < -4;$$

$$(\rho, v, p) = (1 + \varepsilon \sin 5x, 0, 1) \text{ for } x \geq -4.$$

Here we take $\varepsilon = 0.2$. The computed density ρ is plotted at $t = 1.8$ against the “exact solution”, which is a converged solution computed by the fifth order finite difference WENO scheme [5] with 2000 grid points.

In Figures 3.11 and 3.13 we show the results of the CWENO-4 scheme and the CWENO-8 scheme, respectively, using the local characteristic decomposition for the reconstruction from $\{\bar{u}_i^n\}$ to $\{\bar{u}_{i+\frac{1}{2}}^n\}$ and componentwise WENO reconstruction from $\{\bar{u}_i^n\}$ to $\{u_i^n\}$ and componentwise WENO approximation from $\{u_i^n\}$ to $\{f(u)_x|_{x=x_i}\}$. For comparison, we plot the results of the fifth order finite difference WENO scheme using local characteristic decompositions on a non-staggered mesh [5] in Figure 3.12, and the ninth order finite difference WENO scheme using local characteristic decompositions on a non-staggered mesh [1] in Figure 3.14. We can see that higher order schemes give better resolutions to the complex wave patterns after the shock entropy wave interaction, for the same number of grid points. For this problem, the componentwise CWENO and WENO schemes also work very well. We do not show the results to save space.

4 Concluding remarks

In this paper we have developed fourth and eighth order central WENO schemes based on staggered meshes. Negative linear weights appear and they are treated using the recently developed splitting technique of Shi, Hu and Shu [19]. Numerical examples are given to

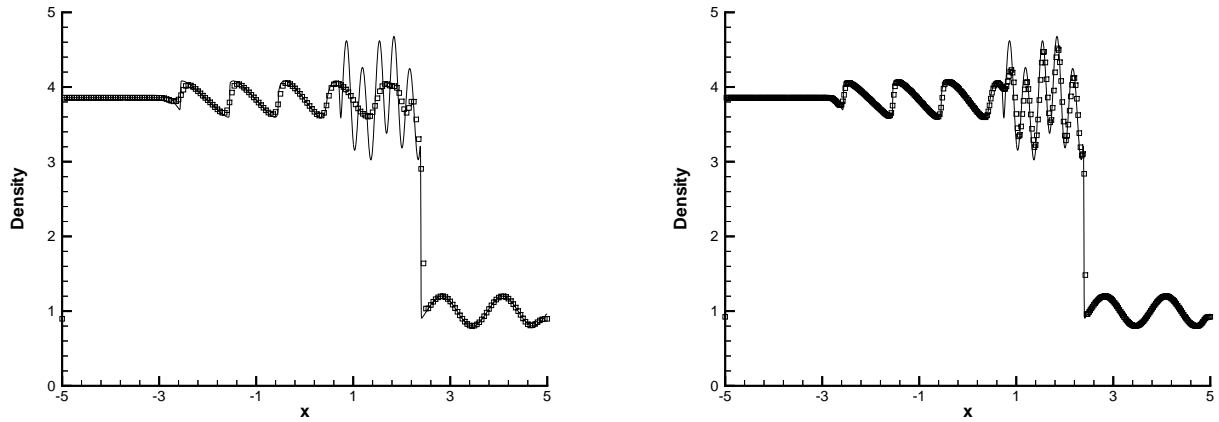


Figure 3.11: The shock density wave interaction problem. $t = 1.8$. CWENO-4 scheme with local characteristic decomposition for the WENO reconstruction of $\bar{u}_{j+\frac{1}{2}}$. Left: $N = 200$ grid points; right: $N = 400$ grid points. Solid line: “exact solution”; squares: computed solution.

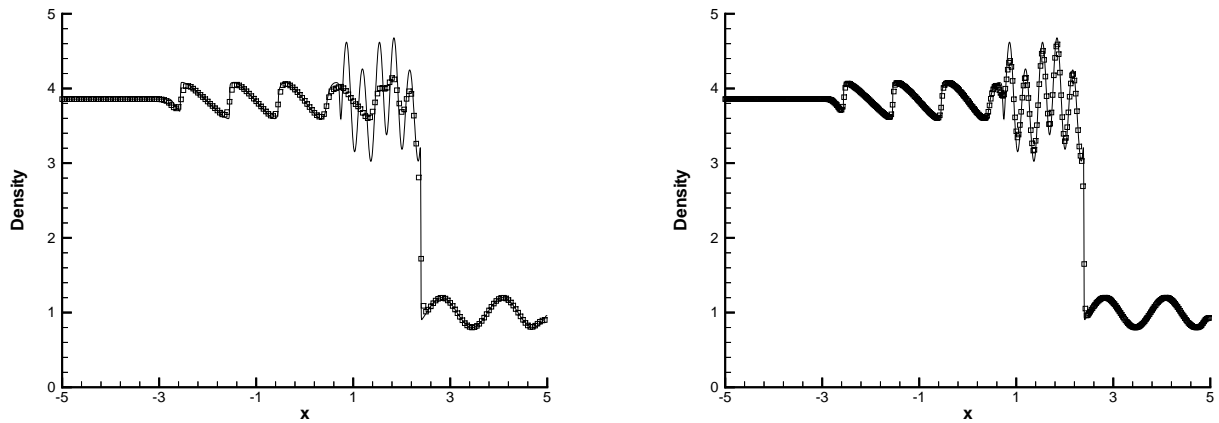


Figure 3.12: The shock density wave interaction problem. $t = 1.8$. WENO-5 finite difference scheme [5] with local characteristic decomposition. Left: $N = 200$ grid points; right: $N = 400$ grid points. Solid line: “exact solution”; squares: computed solution.

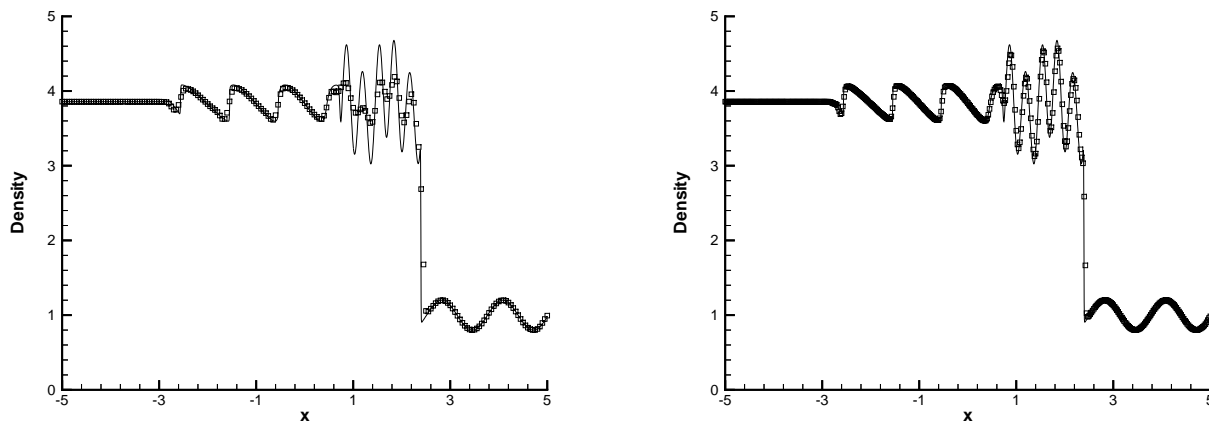


Figure 3.13: The shock density wave interaction problem. $t = 1.8$. CWENO-8 scheme with local characteristic decomposition for the WENO reconstruction of $\bar{u}_{j+\frac{1}{2}}$. Left: $N = 200$ grid points; right: $N = 400$ grid points. Solid line: “exact solution”; squares: computed solution.

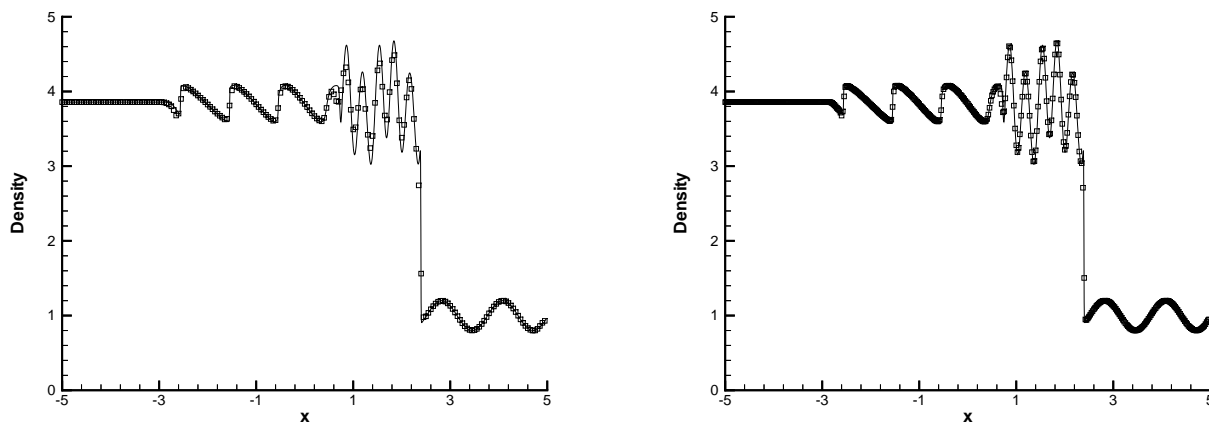


Figure 3.14: The shock density wave interaction problem. $t = 0.16$. WENO-9 finite difference scheme [1] with local characteristic decomposition. Left: $N = 200$ grid points; right: $N = 400$ grid points. Solid line: “exact solution”; squares: computed solution.

verify the order of accuracy of these schemes. Simulations with discontinuous solutions for the Euler equations demonstrate that componentwise WENO reconstruction would yield oscillatory results and the oscillations become more serious with increased order of accuracy, both for the central WENO schemes based on staggered meshes and for the finite difference WENO schemes based on non-staggered meshes [5], [1], although oscillations for the latter are usually more serious. If a local characteristic decomposition is used in the reconstruction, both for the central WENO schemes based on staggered meshes and for the finite difference WENO schemes based on non-staggered meshes, non-oscillatory solutions can be obtained. These high order schemes are useful to simulate problems where shocks and complex smooth regions structures co-exist, such as the problem of shock interaction with entropy waves.

References

- [1] D.S. Balsara and C.-W. Shu, *Monotonicity preserving weighted essentially non-oscillatory schemes with increasingly high order of accuracy*, J. Comput. Phys., 160 (2000), pp. 405-452.
- [2] F. Bianco, G. Puppo and G. Russo, *High-order central schemes for hyperbolic systems of conservation laws*, SIAM J. Sci. Comput., 21 (1999), pp. 294-322.
- [3] A. Harten, B. Engquist, S. Osher and S. Chakravathy, *Uniformly high order accurate essentially non-oscillatory schemes, III*, J. Comput. Phys., 71 (1987), pp. 231-303.
- [4] C. Hu and C.-W. Shu, *Weighted essentially non-oscillatory schemes on triangular meshes*, J. Comput. Phys., 150 (1999), pp. 97-127.
- [5] G.-S. Jiang and C.-W. Shu, *Efficient implementation of weighted ENO schemes*, J. Comput. Phys., 126 (1996), pp. 202-228.
- [6] G.-S. Jiang and E. Tadmor, *Non-oscillatory central schemes for multidimensional hyperbolic conservation laws*, SIAM J. Sci. Comput., 19 (1998), pp. 1892-1917.

- [7] G.-S. Jiang, D. Levy, C.-T. Lin, S. Osher and E. Tadmor, *High-resolution non-oscillatory central schemes with non-staggered grids for hyperbolic conservation laws*, SIAM J. Numer. Anal., 35 (1998), pp. 2147-2168.
- [8] A. Kurganov and D. Levy, *A third-order semidiscrete central scheme for conservation laws and convection-diffusion equations*, SIAM J. Sci Comput., 22 (2000), pp. 1461-1488.
- [9] A. Kurganov and E. Tadmor, *New high-resolution central schemes for nonlinear conservation laws and convection-diffusion equations*, J. Comput. Phys., 160 (2000), pp. 214-282.
- [10] D. Levy, G. Puppo and G. Russo, *Compact central WENO schemes for multidimensional conservation laws*, SIAM J. Sci. Comput., 22 (2000), pp. 656-672.
- [11] D. Levy, G. Puppo and G. Russo, *On the behavior of the total variation in CWENO methods for conservation laws*, Appl. Numer. Math., 33 (2000), pp. 407-414.
- [12] D. Levy, G. Puppo and G. Russo, *A third order central WENO scheme for 2D conservation laws*, Appl. Numer. Math., 33 (2000), pp. 415-421.
- [13] X.D. Liu and S. Osher, *Convex ENO high order multi-dimensional schemes without field by field decomposition or staggered grids*, J. Comput. Phys., 142 (1998), pp. 304-330.
- [14] X.D. Liu and S. Osher, *Nonoscillatory high order accurate self-similar maximum principle satisfying shock capturing schemes I*, SIAM. J. Numer. Anal., 33 (1996), pp. 760-779.
- [15] X.D. Liu and E. Tadmor, *Third order nonoscillatory central scheme for hyperbolic conservation laws*, Numer. Math., 79 (1998), pp. 397-425.
- [16] X.D. Liu, S. Osher and T. Chan, *Weighted essentially non-oscillatory schemes*, J. Comput. Phys., 115 (1994), pp. 200-212.
- [17] H. Nessyahu and E. Tadmor, *Non-oscillatory central differencing for hyperbolic conservation laws*, J. Comput. Phys., 87 (1990), pp. 408-463.

- [18] R. Sanders and A. Weiser, *High resolution staggered mesh approach for nonlinear hyperbolic systems of conservation laws*, J. Comput. Phys., 101 (1992), pp. 314-329.
- [19] J. Shi, C. Hu and C.-W. Shu, *A technique of treating negative weights in WENO schemes*, J. Comput. Phys., to appear.
- [20] C.-W. Shu, *Numerical experiments on the accuracy of ENO and modified ENO schemes*, J. Sci. Comput., 5 (1990), pp. 127-149.
- [21] C.-W. Shu, *Essentially non-oscillatory and weighted essentially non-oscillatory schemes for hyperbolic conservation laws*, in *Advanced Numerical Approximation of Nonlinear Hyperbolic Equations*, B. Cockburn, C. Johnson, C.-W. Shu and E. Tadmor (Editor: A. Quarteroni), Lecture Notes in Mathematics, volume 1697, Springer, 1998, pp. 325-432.
- [22] C.-W. Shu and S. Osher, *Efficient implementation of essentially non-oscillatory shock capturing schemes*, J. Comput. Phys., 77 (1988), pp. 439-471.
- [23] C.-W. Shu and S. Osher, *Efficient implementation of essentially non-oscillatory shock capturing schemes, II*, J. Comput. Phys., 83 (1989), pp. 32-78.
- [24] M. Zennaro, *Natural continuous extensions of Runge-Kutta methods*, Math. Comp., 46 (1986), pp. 119-133.